Optics Letters

How good is your metalens? Experimental verification of metalens performance criterion

Jacob Engelberg,[1] Talia Wildes,[1] Chen Zhou,[2] Noa Mazurski,[1] Jonathan Bar-David,[1] Anders Kristensen,[2] and Uriel Levy[1,*]

[1]Department of Applied Physics, The Center for Nanoscience and Nanotechnology, The Hebrew University, Jerusalem 91904, Israel
[2]Department of Health Technology, Technical University of Denmark, DK-2800 Kongens Lyngby, Denmark
*Corresponding author: ulevy@mail.huji.ac.il

Received 7 April 2020; revised 20 May 2020; accepted 20 May 2020; posted 26 May 2020 (Doc. ID 394680); published 6 July 2020

A metric for evaluation of overall metalens performance is presented. It is applied to determination of optimal operating spectral range of a metalens, both theoretically and experimentally. This metric is quite general and can be applied to the design and evaluation of future metalenses, particularly achromatic metalenses.

https://doi.org/10.1364/OL.394680

Metalenses and diffractive lenses can allow miniaturization and economical mass production of optical systems by replacement of conventional lenses [1–3]. However, many applications require polychromatic operation (i.e., whenever the light source is not a laser), which seemingly cannot be supported by conventionally designed metalenses and diffractive lenses as a result of their strong chromatic aberration [4–6]. This drawback motivates recent research on the development of achromatic metalenses and diffractive lenses [7–12]. Unfortunately, the achromatization usually comes at the expense of reduced efficiency, lens power, and field of view (FOV). On the other hand, it has been shown that nonchromatically corrected metalenses, which we will call from here on "chromatic metalenses," can be used over an extended spectral range, despite the performance degradation resulting from chromatic aberration [13,14]. It therefore becomes important to be able to compare overall performance of different types of metalenses, in order to find an optimal metalens design. In this Letter, we refer to metalenses for conciseness, but the results are equally applicable to diffractive lenses.

In any optical system whose resolution is limited by geometrical aberrations, there is a trade-off between resolution and signal-to-noise ratio (SNR). Decreasing the aperture will reduce aberrations, thus increasing resolution, but will also decrease the number of photons reaching the detector, thus reducing SNR. The overall image quality is determined by the combination of both parameters (resolution and SNR). Since degradation in resolution as a result of aberrations can be compensated by a deconvolution image processing algorithm [15,16], at the expense of added noise, the efficiency and resolution metrics should not be separated.

The above is of course true for metalenses as well. While many reports of metalenses include resolution and efficiency data, these performance metrics are not combined, so it is difficult to compare high-efficiency low-resolution systems (characteristic of a chromatic metalens) to low-efficiency high-resolution systems (characteristic of an achromatic metalens). Therefore, to evaluate overall metalens performance, we must relate to both resolution and SNR and combine the two into a single performance metric. In a previous paper, we proposed an average signal-to-noise ratio (ASNR) metric that fills this gap [17].

The purpose of this Letter is to provide experimental verification of the ASNR metalens performance metric. As a case study, we apply this performance metric to determining the optimal operating spectral range for a chromatic metalens. In the case of a chromatic metalens, the wider the spectral range, the more photons that reach the detector, so the SNR is increased. On the other hand, the chromatic aberration increases too; thus, the resolution is reduced, creating a trade-off between resolution and SNR. By searching for the spectral width that will maximize the ASNR, we can find the optimal operating spectral range for the metalens.

Although this is not discussed further in this Letter, the metric is more general, and can be applied to performance comparison of achromatic metalenses (dispersion engineered or spatially multiplexed) to equivalent chromatic designs. For a spatially multiplexed achromatic metalens—the method can be used to determine the optimal operating spectral range of each channel.

In our previous paper, we theoretically described the ASNR metric and applied it to a generic metalens design [17]. In this Letter, we apply the theory to an actual metalens and compare it to experimental results.

Our measurements were performed on a wide-FOV Huygens metalens, based on a-Si nanodisks on a glass substrate, with a focal length of 3.36 mm and F/2.5 (aperture diameter 1.35 mm), operating around 850 nm wavelength [14]. The metalens uses a simple parabolic phase function, which gives sufficient correction of spherical aberration at F/2.5, and an aperture stop located at the metalens front focal plane, which provides correction of off-axis aberrations [18]. The FOV of the metalens is limited to $\pm 15°$ because of variations in the Huygens nanoantenna angular response.

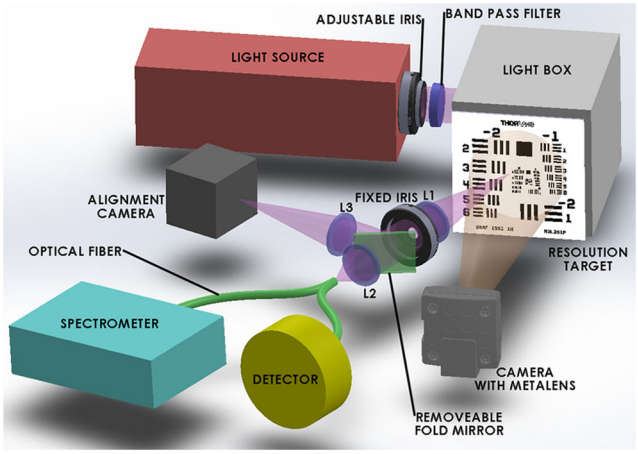

Fig. 1. SNR measurement setup.

The measurement setup shown in Fig. 1 consists of three parts: (1) target projector (from light source to resolution target); (2) device under test, consisting of the metalens coupled to a camera; and (3) spectral radiance meter (from L1 and on toward spectrometer and detector). The target projector is based on a tungsten-halogen lamp (Thorlabs SLS201L), and bandpass filters (BPFs) are used to obtain different spectral widths. The light box serves as an economical alternative to an integrating sphere to provide uniform illumination of the resolution target (Thorlabs R3L3S1P - Positive 1951 USAF Test Target, 3" × 3"), which is imaged onto the camera by the metalens. The adjustable iris is used to adjust the target radiance, so that for all BPFs, we obtain the same peak spectral radiance. The camera used was a Thorlabs DCC1545M monochrome camera (1/2" format, 5.2 μm pixel). The spectrometer (Ocean Insight model FLAME-T-XR1-ES) measures the relative spectral radiance of the target, and the detector (MKS-Ophir StarLite laser power meter with PD300R-UV sensor) measures the absolute total radiance, so together they provide the absolute target spectral radiance (the output end of fiber (Thorlabs M28L01 - Ø400 μm, 0.39 NA) can be switched between spectrometer and detector). The alignment branch of the radiance meter (L3 and alignment camera) allows us to make sure the fiber input is "looking" at the correct area of the target.

Our suggested metric for overall metalens performance is the ASNR, which is the SNR averaged over the relevant spatial frequencies of the image, i.e., from zero to the Nyquist frequency of the camera, as described by Eq. (1) ($f_{\mathrm{nq}} = 1/(2 \cdot \mathrm{pix})$, where pix is the camera pixel pitch) [17]. The SNR that appears outside the integral is the zero (or low) frequency SNR. At higher frequencies, the signal is attenuated by a factor equal to the modulation-transfer-function (MTF) [19] at that frequency, whereas the noise is the same for all frequencies (assuming a shot noise limited system, since shot noise is generally white noise [20]. If this is not the case, the SNR can be placed inside the integral). Therefore, the SNR at any frequency ν is given by the product of SNR at zero spatial frequency and MTF. To obtain the average SNR, we integrate over spatial frequencies up to f_{nq}, and divide by the frequency range,

$$\mathrm{ASNR} = \mathrm{SNR} \int_0^{f_{\mathrm{nq}}} \mathrm{MTF}(\upsilon)\mathrm{d}\upsilon / f_{\mathrm{nq}}. \tag{1}$$

The ASNR can be measured directly or simulated based on system parameters. In the following, we describe how both were done and compare measured to simulated results. This will allow us to experimentally verify the theoretical model. Once the model is verified experimentally, the proposed ASNR metric can be used to evaluate and optimize future metalens designs.

The test setup allows direct SNR measurement, based on the video output from the camera (the camera was characterized to verify linearity and readout + shot noise limited performance, necessary to obtain correct measurements), and simulation of the expected (shot noise limited) SNR based on spectral radiance measurement. We performed the SNR measurements for several spectral widths using BPFs.

The MTF of the metalens for the different spectral ranges was measured using a separate setup, described in [14], and was also simulated using Zemax optical design software. Comparison of measured to simulated MTFs was done previously by the authors [14], but here we integrate the MTFs with the SNR to obtain the ASNR [per Eq. (1)], allowing us to compare simulated to measured overall performance.

The direct SNR measurement is performed by analyzing video images obtained from the metalens when coupled to a video camera. We imaged a resolution target placed 230 mm from the lens, which is the minimum distance at which the spherical aberration is negligible, based on Zemax simulation, so we can use MTF values calculated/measured for a distant object. At this state, we are working with a demagnification of 68×.

We grabbed 30 images, imported them into MATLAB, and measured gray levels of a pixel in the white area and in the black area. The signal is given by the difference between the gray levels, *signal = white level - black level*. The noise is measured by evaluating the standard deviation of the pixel gray level over the 30 images, i.e., temporal rather than spatial noise was measured, to null the effect of any spatial nonuniformity in the target illumination. Thirty images were used since this is the minimum number of samples needed to obtain a good estimate of the standard deviation [21]. To improve the accuracy of the results, the signal and noise were then averaged over many pixels (a few hundred) in each of the areas (black pixels were taken from within the black square on the resolution target, and white pixels were taken from the white area directly to the left of the black square).

To compare the measured noise to simulation, we want to obtain only the shot noise associated with the signal. Therefore, we need to subtract the noise in the black area, which is a result of shot noise from spurious diffraction order photons and readout noise associated with the camera electronics [22]. This is done according to Eq. (2), where σ stands for standard deviation, σ_w is the noise in the white area of the image, σ_b is the noise in the black area, and σ_s the shot noise associated with the signal. The measured SNR is then given by Eq. (3),

$$\sigma_s^2 = \sigma_w^2 - \sigma_b^2, \tag{2}$$

$$\mathrm{SNR} = \mathrm{signal}/\sigma_s. \tag{3}$$

It should be noted that when evaluating an actual metalens design, the contribution of spurious diffraction orders to the noise should be considered, since they reduce the SNR by adding shot noise resulting from the background illumination, but not contributing to the signal. However, for our current

purpose of validating the theoretical model, it is better to measure and subtract this noise, since it is difficult to quantify it theoretically.

The simulated low-frequency SNR is calculated based on the number of photons reaching a camera pixel, assuming a shot noise limited system (this is generally the case for practical modern systems operating in good lighting conditions). The SNR is therefore $\sqrt{N}$ where N is the number of photoelectrons. The radiometric formulas for calculating the number of photoelectrons from the absolute power measured by the detector, the relative spectral distribution measured by the spectrometer, the spectral efficiency of the metalens, the spectral quantum efficiency of the camera, and the parameters of the optical relay system are described in [23]. The simulated SNR is then multiplied by the area under the simulated MTF of the metalens, per Eq. (1), to obtain the simulated ASNR.

In Fig. 2(a), the theoretical ASNR is shown, as a function of spectral range and aperture (the aperture is represented by the $F\#$, defined as $F\# = f/D$, where f is the lens focal length and D is the aperture diameter [24]). This simplified theoretical analysis assumes a Gaussian-shaped spectrum, a wavelength-independent efficiency of the metalens and camera (the spectral range was defined as $2\sqrt{2}\sigma$, where σ is the standard deviation of the Gaussian distribution), and resolution that is limited by chromatic aberration. As can be seen, for lower F#, the optimal operating spectral range is smaller. This can be understood as follows. First, for lower F#, the amount of light collected by the system is larger, so one can afford to improve resolution by reducing the spectral range. In addition, the lower the F#, the larger the chromatic aberration, and this needs to be compensated by reducing the spectral range.

In Fig. 2(b), we show the theoretical ASNR at an aperture of F/2.5 [a slice through the 2D graph of Fig. 2(a), blue], alongside with a more accurate simulated ASNR (red), which takes into account our exact system parameters (measured spectral radiance, metalens and camera spectral efficiency, and simulated on-axis MTF). This is compared with the measured ASNR (yellow), where the SNR was extracted from experimentally captured images produced by our metalens, and the on-axis MTF was taken from measurements performed with our MTF setup. The spectral range of the BPFs was also defined as $2\sqrt{2}\sigma$, where σ is the standard deviation of the spectral distributions.

The results show that the optimum overall performance is obtained at a spectral range of approximately 50 nm (this is independent of the absolute illumination level, which will change the absolute ASNR values, but not its spectral shape). The vertical offset between the simulated and measured results most likely stems from a slight error in calculating the illumination level reaching the camera, which can be caused by inaccuracy in various parameters, e.g., the apertures of the imaging and illumination measurement systems.

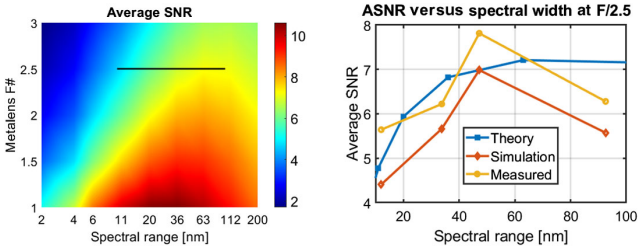

Fig. 2. (a) ASNR vs. F# and spectral range. The black line marks the region where the "Theory" results shown in (b) are taken from. (b) ASNRs at F/2.5: theoretical, simulated, and measured results.

In Fig. 3, the images of the resolution target taken using the metalens coupled to the camera, at different spectral ranges, are shown. These images were purposely taken at low absolute radiance level and short camera exposure time [25 W/(m^2·nm) and 1.23 ms, respectively]. The peak spectral radiance was kept constant for all spectral widths, by varying the adjustable iris to compensate for variations in BPF peak transmission. This simulates the real-life scenario of choosing different spectral widths with which to view a scene. While, as previously mentioned, the absolute illumination does not affect the optimal spectral range, for the qualitative demonstration shown in Fig. 3, it is necessary to operate at low light level, in order to obtain low SNRs that are visually distinguishable.

Looking at the raw images [Figs. 3(a)–3(c)], one can see that the 100 nm spectral range image is the blurriest, because of the large chromatic aberration, but less noisy. The 10 nm spectral range image is sharpest, but quite noisy. The 50 nm spectral range image provides a convenient compromise between the two. Following Weiner deconvolution [15] [Figs. 3(d)–3(f)], the resolution of the blurry images is improved, at the expense of added noise. The 50 nm spectral range image still gives the best quality, as a compromise between resolution and noise. As a result of the low light level used, camera readout noise is visible in the 10 nm bandwidth images, but this noise is subtracted out of the calculated ASNR [Eq. (2)], so it does not impact the "measured" graph in Fig. 2(b).

In order to facilitate the use of our ASNR metric in the design stage of a metalens, it is important to clarify whether our simulation can also provide qualitative image rendering that will give an indication of the expected image quality for a given design. To this end, we used a high-quality image of a resolution target like the one used in the measurement. We then applied to it the simulated MTF (from Zemax) and noise (the square-root of the number of photoelectrons, calculated based on the spectral radiance and exposure time mentioned above, integrated over the different spectral ranges). The result is shown in Fig. 4.

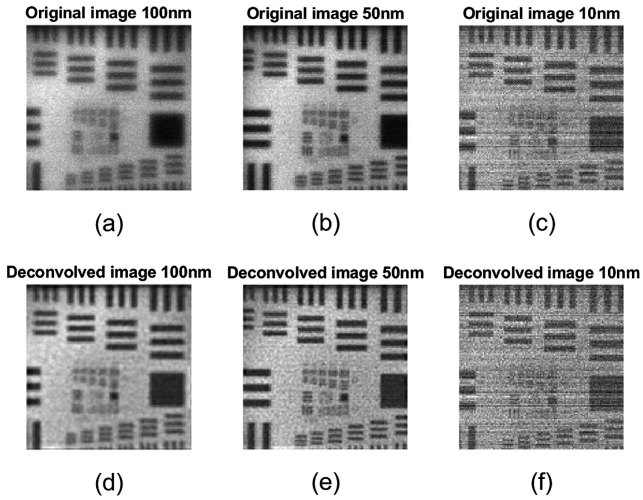

Fig. 3. (a)–(c) Measured images at spectral ranges of 100 nm, 50 nm, and 10 nm, respectively. (d)–(e) Same as the above, following Weiner deconvolution. FOV shown is 10°.

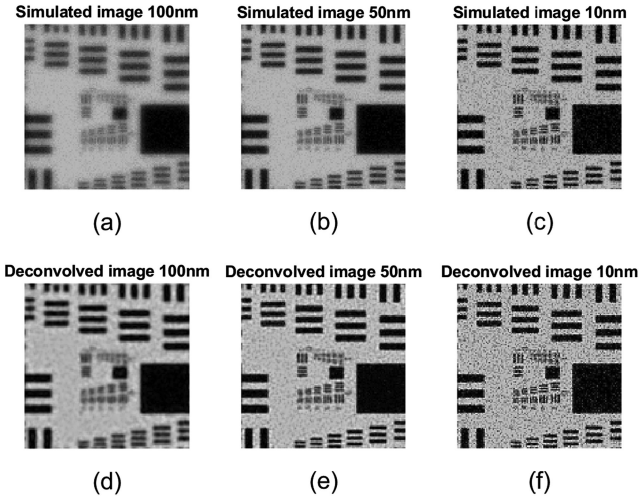

Fig. 4. (a)–(c) Simulated images at spectral ranges of 100 nm, 50 nm, and 10 nm, respectively. (d)–(e) Same as the above, following Weiner deconvolution.

The simulated images of Fig. 4 resemble the measured images (Fig. 3), with two main differences. The first difference is the low-frequency contrast, i.e., how black the large black areas are (known as "veiling glare" [25]). This is because in our simulation we did not account for the light transmitted to other diffraction orders. This can, of course, be added to the simulation artificially, if the level of veiling glare is known from simulation or measurement. Conversely, following the deconvolution process, the contrast of the real images can be enhanced by subtracting the black level from them (and then multiplying by an appropriate gain constant to raise the white level back up—this will of course increase the noise proportionally, so the SNR remains constant), thus obtaining a match with the simulated images. An additional difference between the real and simulated images is visible mostly in the 10 nm spectral width [Figs. 3(c) and 3(f) versus Figs. 4(c) and 4(f), respectively]. In the real images, camera readout noise is visible, in the form of horizontal lines, while it is of course absent in the simulated images. This is not a serious impediment, since in most real-world scenarios one does not operate at such low light level/short exposure times.

In conclusion, we have experimentally validated a theoretical method for evaluating the overall performance of a metalens system. The approach can work equally well for a diffractive lens system. This method can be used to optimize operating spectral range of a chromatic or achromatic metalens design. It can also be used to compare performance of different designs, such as achromatic versus equivalent chromatic flat lens designs.

Funding. Ministry of Science, Technology and Space.

Disclosures. The authors declare no conflicts of interest.

REFERENCES

1. P. Lalanne and P. Chavel, Laser Photon. Rev. **11**, 1600295 (2017).
2. M. Khorasaninejad and F. Capasso, Science **358**, eaam8100 (2017).
3. M. L. Tseng, H. H. Hsiao, C. H. Chu, M. K. Chen, G. Sun, A. Q. Liu, and D. P. Tsai, Adv. Opt. Mater. **6**, 1800554 (2018).
4. D. D. O'Shea, T. J. Suleski, A. D. Kathman, and D. W. Praather, *Diffractive Optics* (SPIE, 2003).
5. E. Arbabi, A. Arbabi, S. M. Kamali, Y. Horie, and A. Faraon, Optica **3**, 628 (2016).
6. M. Khorasaninejad, A. Zhu, C. Roques-Carmes, W. T. Chen, J. Oh, I. Mishra, and R. C. Devlin, Nano Lett. **16**, 7229 (2016).
7. S. Shrestha, A. C. Overvig, M. Lu, A. Stein, and N. Yu, Light Sci. Appl. **7**, 85 (2018).
8. N. Mohammad, M. Meem, B. Shen, P. Wang, and R. Menon, Sci. Rep. **8**, 2799 (2018).
9. S. Banerji, M. Monjurul, A. Majumder, F. G. Vasquez, B. Sensale-Rodriguez, and R. Menon, Optica **6**, 805 (2019).
10. M. Khorasaninejad, Z. Shi, A. Y. Zhu, W. T. Chen, V. Sanjeev, A. Zaidi, and F. Capasso, Nano Lett. **17**, 1819 (2017).
11. W. T. Chen, A. Y. Zhu, V. Sanjeev, M. Khorasaninejad, Z. Shi, E. Lee, and F. Capasso, Nat. Nanotechnol. **13**, 220 (2018).
12. S. Colburn, A. Zhan, and A. Majumdar, Sci. Adv. **4**, eaar2114 (2018).
13. M. Khorasaninejad, W. T. Chen, R. C. Devlin, J. Oh, A. Y. Zhu, and F. Capasso, Science **352**, 1190 (2016).
14. J. Engelberg, C. Zhou, N. Mazurski, J. Bar-David, A. Kristensen, and U. Levy, Nanophotonics **9**, 361 (2020).
15. R. C. González and R. E. Woods, *Digital Image Processing*, 2nd ed. (Prentice Hall, 2002).
16. R. Zanella, G. Zanghirati, R. Cavicchioli, L. Zanni, P. Boccacci, M. Bertero, and G. Vicidomini, Sci. Rep. **3**, 2523 (2013).
17. J. Engelberg and U. Levy, Opt. Express **25**, 21637 (2017).
18. D. A. Buralli and G. M. Morris, Appl. Opt. **28**, 3950 (1989).
19. G. D. Boreman, *Modulation Transfer Function in Optical and Electro-Optical Systems* (SPIE, 2001).
20. D. Bagrets and F. Pistolesi, Phys. E **40**, 123 (2007).
21. R. E. Walpole, R. H. Myers, S. L. Myers, and K. Ye, *Probability and Statistics for Engineers and Scientists*, 8th ed. (Pearson Prentice Hall, 2007).
22. G. C. Holst and T. S. Lomheim, *CMOS/CCD Sensors and Camera Systems* (SPIE, 2011).
23. J. Engelberg, T. Wildes, C. Zhou, N. Mazurski, J. Bar-David, A. Kristensen, and U. Levy "How good is your metalens? Experimental verification of metalens performance criterion," arXiv:2002.07425v1 (2020).
24. W. J. Smith, *Modern Optical Engineering*, 3rd ed. (McGraw-Hill, 2000).
25. I. Tomić, I. Karlović, and I. Jurič, J. Graph. Eng. Des. **5**, 23 (2014).